Title

Gamma distribution model of diffusion MRI for evaluating the isocitrate dehydrogenase mutation status of glioblastomas.

Journal

British Journal of Radiology, 95(1133)

Authors

Takase, Hanae
Togao, Osamu
Kikuchi, Kazufumi
et al.

Publication Date

2022-05-01

DOI

10.1259/bjr.20210392

Peer reviewed

BJR

https://doi.org/10.1259/bjr.20210392

Received: 27 March 2021 | Revised: 25 December 2021 | Accepted: 28 January 2022 | Published online: 08 February 2022

Cite this article as:
Takase H, Togao O, Kikuchi K, Hata N, Hatae R, Chikui T, et al. Gamma distribution model of diffusion MRI for evaluating the isocitrate dehydrogenase mutation status of glioblastomas. *Br J Radiol* (2022) 10.1259/bjr.20210392.

FULL PAPER

Gamma distribution model of diffusion MRI for evaluating the isocitrate dehydrogenase mutation status of glioblastomas

[1]HANAE TAKASE, [2]OSAMU TOGAO, [1]KAZUFUMI KIKUCHI, [3]NOBUHIRO HATA, [3]RYUSUKE HATAE, [4]TORU CHIKUI, [5]KENJI TOKUMORI, [4]YUKIKO KAMI, [3]DAISUKE KUGA, [3]YUHEI SANGATSUDA, [3]MASAHIRO MIZOGUCHI, [1]AKIO HIWATASHI and [1]KOUSEI ISHIGAMI

[1]Department of Clinical Radiology, Graduate School of Medical Sciences, Kyushu University, Fukuoka, Japan
[2]Department of Molecular Imaging & Diagnosis, Graduate School of Medical Sciences, Kyushu University, Fukuoka, Japan
[3]Department of Neurosurgery, Graduate School of Medical Sciences, Kyushu University, Fukuoka, Japan
[4]Department of Oral and Maxillofacial Radiology, Faculty of Dental Science, Kyushu University, Fukuoka, Japan
[5]Department of Clinical Radiology, Faculty of Medical Technology, Teikyo University, Fukuoka, Japan

Address correspondence to: Dr Osamu Togao
E-mail: *togao.osamu.595@m.kyushu-u.ac.jp*

Objective: To determine whether the γ distribution (GD) model of diffusion MRI is useful in the evaluation of the isocitrate dehydrogenase (IDH) mutation status of glioblastomas.

Methods: 12 patients with IDH-mutant glioblastomas and 54 patients with IDH-wildtype glioblastomas were imaged with diffusion-weighted imaging using 13 b-values from 0 to 1000 s/mm^2. The shape parameter (κ) and scale parameter (θ) were obtained with the GD model. Fractions of three different areas under the probability density function curve (f1, f2, f3) were defined as follows: f1, diffusion coefficient (D) < 1.0×10^{-3} mm^2/s; f2, $D > 1.0\times10^{-3}$ and $<3.0\times10^{-3}$ mm^2/s; f3, $D > 3.0\times10^{-3}$ mm^2/s. The GD model-derived parameters measured in gadolinium-enhancing lesions were compared between the IDH-mutant and IDH-wildtype groups. Receiver operating curve analyses were performed to assess the parameters' diagnostic performances.

Results: The IDH-mutant group's f1 (0.474 ± 0.143) was significantly larger than the IDH-wildtype group's (0.347 ± 0.122, $p = 0.0024$). The IDH-mutant group's f2 (0.417 ± 0.131) was significantly smaller than the IDH-wildtype group's (0.504 ± 0.126, $p = 0.036$). The IDH-mutant group's f3 (0.109 ± 0.060) was significantly smaller than the IDH-wildtype group's (0.149 ± 0.063, $p = 0.0466$). The f1 showed the best diagnostic performance among the GD model-derived parameters with the area under the curve value of 0.753.

Conclusion: The GD model could well describe the pathological features of IDH-mutant and IDH-wildtype glioblastomas, and was useful in the differentiation of these tumors.

Advances in knowledge: Diffusion MRI based on the γ distribution model could well describe the pathological features of IDH-mutant and IDH-wildtype glioblastomas, and its use enabled the significant differentiation of these tumors. The γ distribution model may contribute to the non-invasive identification of the IDH mutation status based on histological viewpoint.

INTRODUCTION

Glioblastoma is the most common primary brain neoplasm, accounting for 15% of all intracranial neoplasms and 46% of malignant primary brain tumors.[1] Glioblastomas are highly aggressive astrocytomas which are resistant to therapy and thus have a corresponding poor prognosis. One of the most important prognostic biomarkers in glioma patients is the patients' isocitrate dehydrogenase (IDH) mutation status. In the 2016 World Health Organization classification system, glioblastomas are subdivided into two types on the basis of the presence of IDH mutation.[2] Among patients with glioblastomas, those with IDH-mutant tumors have shown significantly better overall survival compared to those with IDH-wildtype tumors.[3] Although genetic analyses following surgical resections or biopsies are considered the reference standard for evaluations of the IDH mutation status, resections and biopsies are invasive, and in gliomas, they are affected by inherent sampling errors associated with intratumoral histological heterogeneity. A non-invasive imaging method that can predict the IDH mutation status of glioblastomas is thus desired.

Several diffusion MRI studies have evaluated the IDH mutation status of glioblastomas, but in those studies, the apparent diffusion coefficient (ADC) was reported to be either lower[4] or higher in IDH-mutant glioblastomas than in IDH-wildtype glioblastomas,[5,6] and another study reported that there was no difference between these groups.[7] A consensus regarding the usefulness of diffusion MRI in diagnosing the IDH mutation status has thus not been obtained.

A statistical model based on the γ distribution (GD) has been proposed as one of the non-Gaussian distribution models for diffusion MRI analyses.[8] The GD model is a two-parameter family of continuous probability distributions parametrized in terms of the shape parameters κ (κ) and the scale parameter θ (θ), and this model assumes that the diffusion coefficient (D) is distributed continuously within a voxel. The GD model allows the estimations of fractions of a tissue type based on the concept that the area fractions for $D < 1.0\times10^{-3}$ mm^2/s, 1.0×10^{-3} to 3.0×10^{-3} mm^2/s, and $D > 3.0\times10^{-3}$ mm^2/s are attributed to intracellular, extracellular extravascular, and intravascular spaces, respectively.[8] The GD model is suitable for realistically interpreting diffusion data in a histological context. The GD model has been used to assess prostate cancers[8–10] and breast cancers.[11] To the best of our knowledge, there has been only one study to date on the application of the GD model to brain tumors, by Togao et al who investigated its usefulness in differentiating glioblastomas from malignant lymphomas.[12] We conducted the present study to evaluate the usefulness and diagnostic performance of GD model-derived parameters in the differentiation of IDH-mutant and IDH-wildtype glioblastomas.

METHODS AND MATERIALS

This retrospective study was approved by the Institutional Review Board of Kyushu University Hospital (no. 2019–447), and the requirement for informed consent was waived.

Patients

Multi-b-value diffusion MRI has been a part of our routine preoperative MRI protocol for patients with brain tumors since January 2013. The patient inclusion criteria for this study were: (1) multi-b-value diffusion MRI was conducted pre-operatively for the patient during the period from January 2013 to August 2019; and (2) the patient subsequently underwent a surgical resection or biopsy within 1 month of the imaging, and the histopathological diagnosis of glioblastoma was made. A total of 71 patients met these criteria. The exclusion criteria were as follows: (1) no distinct contrast enhancement observed in the lesion (n = 5), and (2) the analysis of the patient's images was difficult due to severe artifacts (n = 0). Thus, a total of 66 patients with glioblastomas were identified. Subsequent genetic analyses revealed that 12 patients (mean age 37.5 ± 8.5 years, range 23–51 years) had IDH-mutant glioblastomas and 54 patients (mean age 67.4 ± 14.7 years, range 17–87 years) had IDH-wildtype glioblastomas.

MRI

All MR images were obtained by a 3T MRI unit (Achieva 3.0 T TX/Ingenia 3.0T; Philips Healthcare, Best, The Netherlands) with an 8- or 15-channel head coil. The diffusion MRI was performed in axial planes by using a single-shot echoplanar imaging diffusion sequence, with 13 b-values (0, 10, 20, 30, 50, 80, 100, 200, 300, 400, 600, 800, and 1000 s/mm^2) in three orthogonal directions. The other imaging parameters were: repetition time, 2500 ms; echo time, 70 ms; matrix, 128 × 126 (reconstructed to 256 × 256); slice thickness, 5 mm, field of view, 230 × 230 mm; number of slices, 11; sensitivity encoding factor, 1.5; scan time, 2 min 7 s. For reference, several standard MR images including T_1 weighted, T_2 weighted, fluid-attenuated inversion recovery (FLAIR), and contrast-enhanced T_1 weighted images were acquired.

Image analysis

The GD model is represented by P(D) and given by:

$$\rho(D) = \frac{1}{\Gamma(k)\theta^k} \cdot D^{k-1} \cdot exp\left(\frac{-D}{\theta}\right) \quad (1)$$

where κ is the shape parameter related to the statistical dispersion of the diffusion coefficient (D) distribution, and θ is the scale parameter for this dispersion. If the κ is small, the resulting GD probability density function (PDF) curve will be right-skewed, and if the κ is large, the resulting PDF curve will be left-skewed. If the θ is large, the resulting PDF will be broad. The parameters κ and θ were estimated by a curve-fitting of the signal intensities obtained at the 13 b-values by the following equation:

$$S(b) = S0 \cdot \frac{1}{(1+\theta b)^k} \quad (2)$$

where Sb is the signal intensity for each b-value and S0 is the signal intensity at a b-value of zero.

Three different areas under the PDF curve are defined as follows: f1, the area fraction of D smaller than 1.00×10^{-3} mm^2/s; f2, the area fraction of D from 1.00×10^{-3} mm^2/s to 3.00×10^{-3} mm^2/s; f3, the area fraction of diffusion larger than 3.00×10^{-3} mm^2/s. The f1 value is attributed to the intracellular component; the f2 is attributed to the extracellular extravascular component, and the f3 is attributed to the intravascular component.[8]

The diffusion MRI data in the Digital Imaging and Communications in Medicine (DICOM) format were transferred to a personal computer and fit to the GD model, and then the κ and θ values were estimated using the Image J software program (v. 1.52p; U.S. National Institutes of Health, Bethesda, MD) and self-built plug-ins. After the export of the x- and y-coordinates and the κ and θ of each pixel within the region of interest (ROI), the f1, f2, and f3 values of each pixel were calculated using Microsoft Excel v. 16.16.14.

ADC values were also computed with the monoexponential model using all of the above-listed 13 b-values (0, 10, 20, 30, 50, 80, 100, 200, 300, 400, 600, 800, and 1000 sec/mm^2) according to the following equation:

$$\frac{S_b}{S_0} = e^{-b\times ADC} \quad (3)$$

Figure 1. Region of interest (ROIs). (**A**) On post-contrast T_1 weighted images, areas showing contrast enhancement were manually segmented (*red ROI*). The areas with necrosis, cystic lesion, hemorrhage, or obvious artifacts were carefully excluded from the ROI. (**B**) The ROIs were copied from the post-contrast T_1 weighted images and pasted to the b-value of the 0 s/mm^2 image. ROIs were also placed on the non-contrast-enhancing peritumoral T2-hyperintense area on the image obtained with the b-value of 0 s/mm^2 (*blue ROI*). ROI, region of interest.

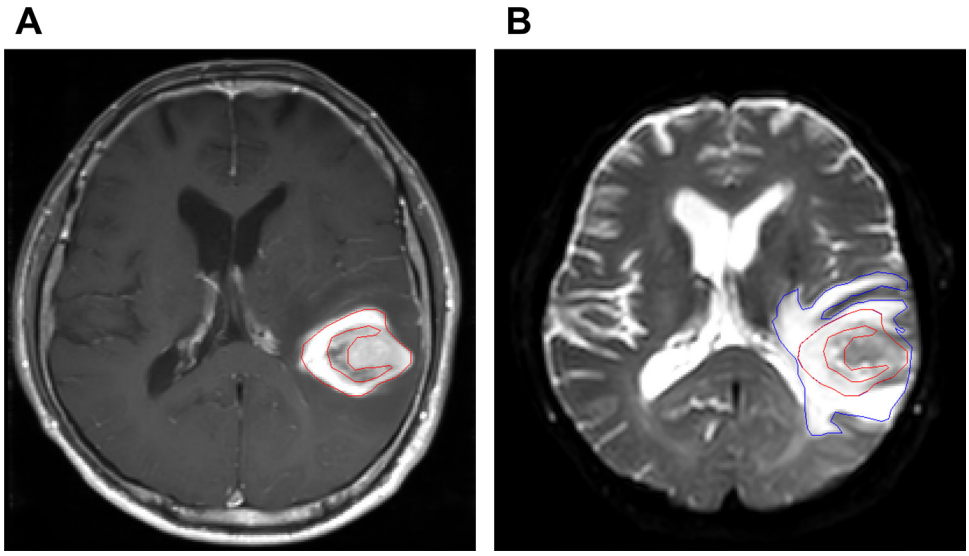

where Sb is the signal intensity for each b-value and S0 is the signal intensity at a b-value of zero.

ROI placement

We adjusted the matrix sizes of the postcontrast T_1 weighted images to the same size as those of the diffusion MRI images by using the ImageJ function to match the geometric information of these images. No image registration algorithm was used in this study. We then placed ROIs to delineate the gadolinium-enhancing lesion on the single slice that had the maximum area on the size-adjusted postcontrast T_1 weighted images. The ROIs were manually segmented by a radiologist (HT with 2 years' experience). A board-certified radiologist (OT 21 years' experience) approved the segmentation (Figure 1A). The areas with necrosis, cystic lesion, hemorrhage, or obvious artifacts were carefully excluded from the ROI.

The ROIs were copied from the post-contrast T_1 weighted images and pasted to the b-value of the 0 s/mm^2 image (Figure 1B). Fine manual adjustments were made when there were locational mismatches due to image distortion or the patient's motion. ROIs were also placed on the non-contrast-enhancing peritumoral T2-hyperintense areas as well as on the contralateral normal-appearing white matter on the image obtained with the b-value of the 0 s/mm^2 image. The ROI sizes for the contrast-enhancing areas, non-contrast-enhancing peritumoral T2-hyperintense areas, and contralateral normal-appearing white matter were 606 ± 611, 335 ± 244, and 202 ± 102 mm^2, respectively. The largest possible oval ROI was placed in the contralateral normal-appearing white matter in each patient.

Molecular pathology

The samples were obtained from all patients during the surgery. The IDH mutation status of each glioblastoma was identified in all patients including younger patients by the deoxyribonucleic acid sequencing method as described.[13] Immunohistochemistry was performed clinically in all cases but was not used as a method to determine IDH mutation in this study.

Statistical analyses

The mean values of the GD model-derived parameters and ADCs measured in the ROIs were obtained and then compared between the IDH-mutant and IDH-wildtype glioblastoma groups with the unpaired *t*-test. A receiver operating characteristic curve (ROC) analysis was performed to assess the diagnostic performance of the parameters in this differentiation. The area under the curve (AUC) was calculated, and then the sensitivity and specificity were obtained. The optimal cut-off point was determined by Youden's method. The diagnostic performance was considered excellent for AUC values between 0.9 and 1.0, good for AUC values between 0.8 and 0.9, fair for those between 0.7 and 0.8, poor for those between 0.6 and 0.7, and failed for those between 0.5 and 0.6.[14] Two independent AUCs were compared using the method of Delong et al.[15] We examined the correlations between ADC and the GD-derived fractions (f1, f2, f3) using Pearson's correlation coefficient to investigate the influence of each histological component on ADC in each tumor. Statistical analyses were performed with Prism 5.0 (GraphPad Software, San Diego, CA), MedCalc 19.1 (Broekstraat, Mariakerke, Belgium), and JMP Pro 14.0 (SAS Institute, Cary, NC). The results with a *p*-value <0.05 were considered significant.

RESULTS

Comparisons of the GD-derived parameters between the IDH-mutant and IDH-wildtype groups

Figure 2 illustrates the results of our comparisons of the GD model-derived parameters in the gadolinium-enhancing

Figure 2. Comparisons of the GD model-derived parameters between the IDH-mutant and IDH-wildtype glioblastomas among the gadolinium-enhancing lesions. (**A**) The κ values tended to be smaller in the IDH-mutant group compared to the IDH-wildtype group, the difference was not significant. (**B**) The θ was not significantly different between the groups. (**C–E**) The f1 was significantly larger and the f2 and f3 were significantly smaller in the IDH-mutant group than in the IDH-wildtype group. GD, γ distribution; IDH, isocitrate dehydrogenase.

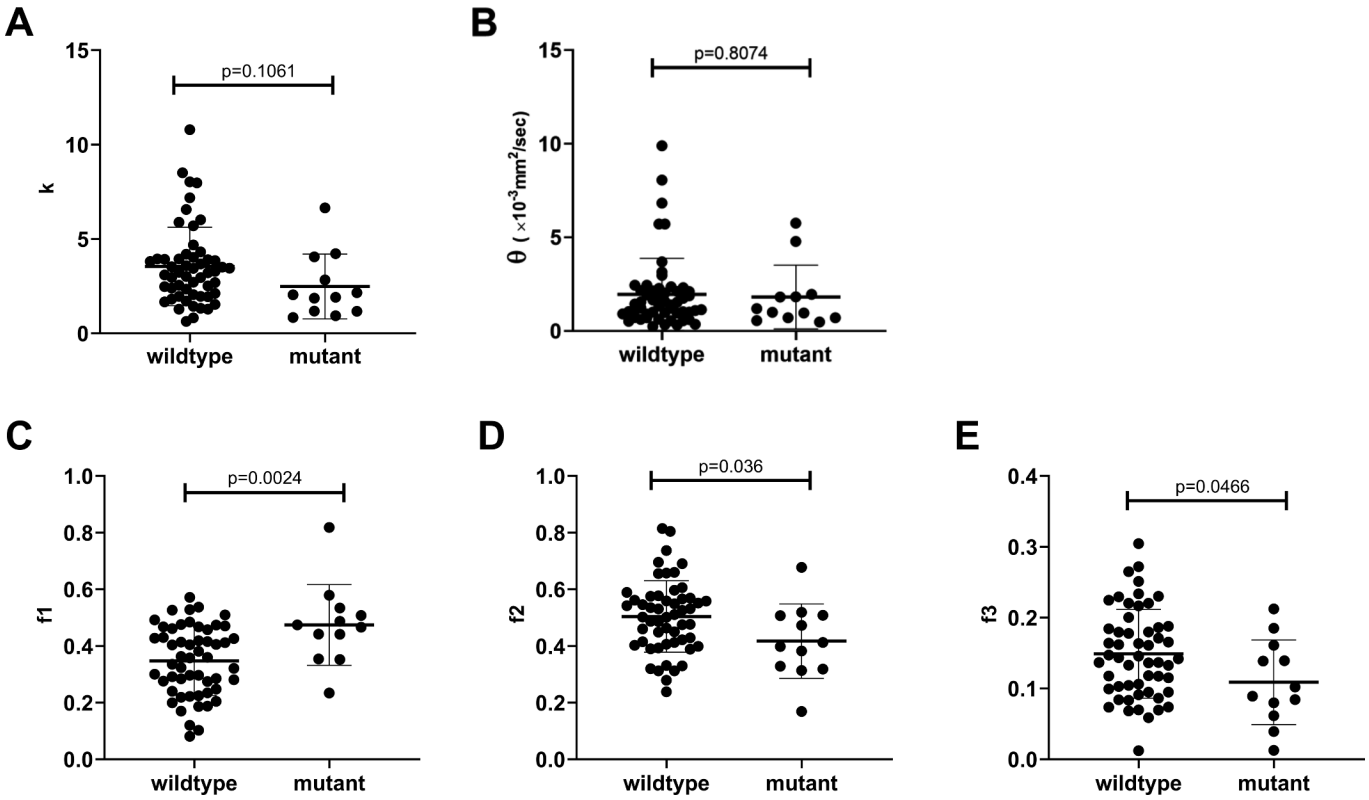

lesions between the IDH-mutant and IDH-wildtype groups. Although the κ values tended to be smaller in the IDH-mutant group compared to the IDH-wildtype group, the difference was not significant. There was no significant difference in the θ values between the IDH mutant and IDH-wildtype groups. The f1 was significantly larger in the IDH-mutant group (0.474 ± 0.143, p = 0.0024) than in the IDH-wildtype group (0.347 ± 0.122). The f2 was significantly smaller in the IDH-mutant group (0.417 ± 0.131, p = 0.036) than in the IDH-wildtype group (0.504 ± 0.126). The f3 was significantly smaller in the IDH-mutant group (0.109 ± 0.060, p = 0.047) than in the IDH-wildtype group (0.149 ± 0.063). The ADC value of the enhancing lesion was significantly smaller in the IDH-mutant group (1.04 ± 0.24×10^{-3} mm^2/s) than in the IDH-wildtype group (1.25 ± 0.28×10^{-3} mm^2/s, p = 0.018). The detailed information for the parameters is summarized in Table 1.

In the peritumoral T2-hyperintense areas without contrast enhancement, no significant differences were observed between the IDH-mutant and -wildtype groups for any of the GD model-derived parameters.

Figure 3 provides a representative IDH-mutant glioblastoma case. The gadolinium-enhancing lesion shows a low κ, a large f1, a small f2, and a small f3, suggesting IDH-mutant status. Figure 4 demonstrates a representative case of IDH-wildtype

Table 1. γ distribution model-derived parameters in IDH-mutant and IDH-wildtype glioblastomas

		κ	θ,×10^{-3} mm^2/s	f1	f2	f3
Enhancing lesion	Mutant	2.49 ± 1.72	1.82 ± 1.71	0.474 ± 0.143	0.417 ± 0.131	0.109 ± 0.060
	Wildtype	3.55 ± 2.08	1.96 ± 1.93	0.347 ± 0.122	0.504 ± 0.126	0.149 ± 0.063
Peritumoral T2-hyperintense area	Mutant	7.60 ± 3.37	0.54 ± 0.57	0.159 ± 0.107	0.762 ± 0.109	0.079 ± 0.044
	Wildtype	8.25 ± 3.11	0.41 ± 0.26	0.193 ± 0.151	0.747 ± 0.128	0.074 ± 0.041
NAWM	Mutant	2.51 ± 1.05	2.10 ± 4.29	0.627 ± 0.049	0.318 ± 0.054	0.056 ± 0.042
	Wildtype	3.05 ± 2.10	1.06 ± 1.46	0.556 ± 0.138	0.388 ± 0.128	0.056 ± 0.024

IDH, isocitrate dehydrogenase; NAWM, normal appearing white matter.

Figure 3. A 23-year-old-male with an IDH-mutant glioblastoma. (**A**) The post-contrast T_1 weighted image shows a solid enhancing lesion in the left frontal lobe (*arrow*). The enhancing lesion shows high signal intensity on the diffusion-weighted image at the b-value of 1000 s/mm^2 (**B**) and a low ADC (0.56 × 10^{-3} mm^2/s, (**C**). This lesion shows a small κ (2.83, (**D**), a small θ (0.56 × 10^{-3} mm^2/s, (**E**), a large f1 (0.818, (**F**), a small f2 (0.169, (**G**), and a small f3 (0.013, (**H**)). ADC, apparent diffusion coefficient; IDH, isocitrate dehydrogenase.

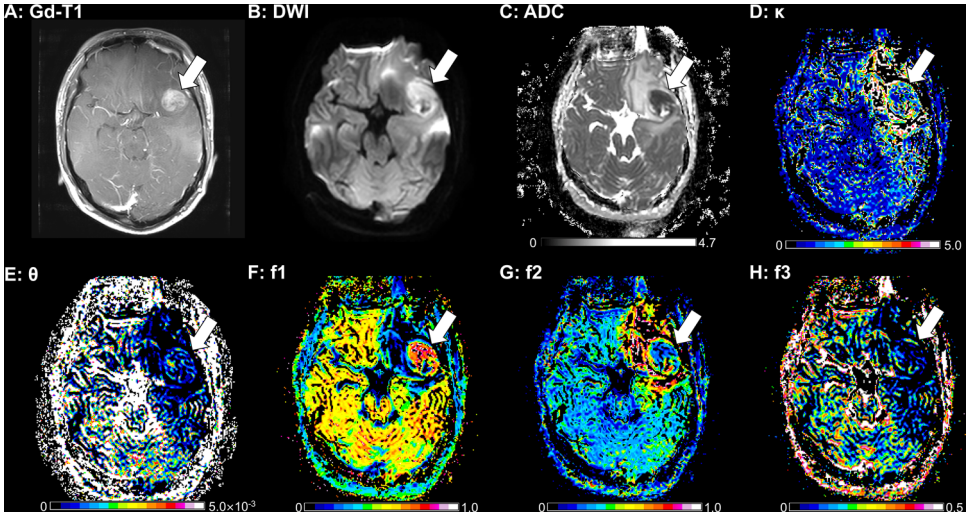

glioblastoma. The enhancing lesion shows a large κ, a small f1, a large f2, and a large f3, which are consistent with the IDH-wildtype status.

Diagnostic performance of the GD model-derived parameters

The ROC graphs and diagnostic performance parameters are provided in Figure 5 and Table 2. In the analysis regarding the differential diagnosis of IDH-mutant and -wildtype glioblastomas, the f1 and ADC showed fair performances; f2, f3, and κ showed poor performances, and the θ resulted in a failed performance. The f1 provided the highest AUC value at 0.753, and the ADC value showed a comparable AUC at 0.733. The f3 demonstrated a significantly higher AUC value than the θ (p = 0.0216). Otherwise, no significant differences were revealed in the comparisons of the ROC curves among the parameters.

Correlations of the GD model-derived parameters with the ADC

Figure 6 illustrates the correlations between the ADC and f1, f2, and f3 in the IDH-mutant and -wildtype groups. Very strong negative correlations between f1 and ADC were observed in both the IDH-mutant (r= −0.9792, $p < 0.0001$) and IDH-wild-type groups (r= −0.8641, $p < 0.0001$). Very strong and strong positive

Figure 4. A 69-year-old-male with an IDH-wildtype glioblastoma. (**A**) The post-contrast T_1 weighted image shows an irregular enhancing lesion in the left basal ganglia (*arrow*). The enhancing lesion shows low signal intensity on the diffusion-weighted image at the b-value of 1000 s/mm^2 (**B**) and a high ADC (1.66 × 10^{-3} mm^2/s, (**C**). This lesion shows a large κ (3.28) (**D**), a large θ (1.75 × 10^{-3} mm^2/s, (**E**), a small f1 (0.186) (**F**), a moderate f2 (0.549) (**G**), and a large f3 (0.265) (**H**). ADC, apparent diffusion coefficient; IDH, isocitrate dehydrogenase.

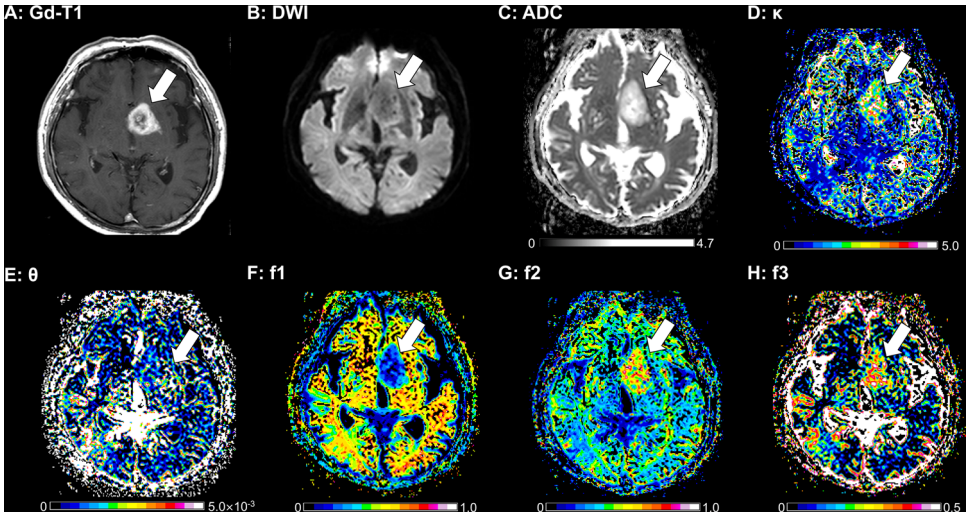

Figure 5. ROC graphs for the differentiation of IDH-mutant and IDH-wildtype glioblastomas. The f1 and ADC showed fair performances, whereas f2, f3, and κ showed poor performances, and the θ resulted in a failed performance. The f1 showed the highest AUC value at 0.753. ADC, apparent diffusion coefficient; AUC, area under the curve; IDH, isocitrate dehydrogenase; ROC, receiver operating characteristic.

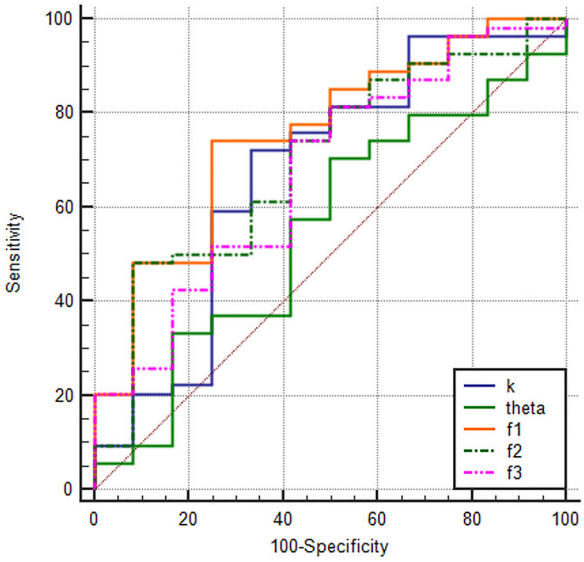

correlations between f2 and ADC were observed in the IDH-mutant (r = 0.9266, p < 0.0001) and IDH-wildtype (r = 0.6925, p < 0.0001) groups, respectively. A weak positive correlation between f3 and ADC was observed in the IDH-wildtype group (r = 0.2899, p = 0.0335), whereas no significant correlation was observed in the IDH-mutant group (r = 0.3026, p = 0.3390).

DISCUSSION

The results of our analyses demonstrated that compared to the IDH-wildtype tumors, the IDH-mutant glioblastomas had larger f1, smaller f2, and smaller f3 in the enhancing lesions. The ROC analyses for the differentiation of both groups revealed that the f1 showed the highest diagnostic performance among the GD model-derived parameters. The ADC was significantly correlated with the f1 and f2 in both groups and was correlated with the f3 in the IDH-wildtype group.

Histologically, glioblastomas are highly cellular gliomas that are usually composed of poorly differentiated tumor cells with nuclear atypia and mitotic activity.[16] Microvessel proliferation and necrosis are essential features. The larger f1 and smaller f2 observed in the present IDH-mutant glioblastomas compared to the IDH wild-type glioblastomas indicated that IDH-mutant glioblastomas had higher cell density and a smaller fraction of interstitial space. These results are reasonable since it is known that IDH-mutant glioblastomas histologically have less macroscopic and microscopic necrosis compared to IDH-wildtype glioblastomas.[16] Microscopically, areas of ischemic and/or palisading necrosis were observed in 50.0% of IDH-mutant glioblastomas, a significantly lower percentage than in IDH-wildtype glioblastomas (90.3%).[17] The lower frequency of microscopic necrosis in IDH-mutant glioblastomas might explain our present findings regarding f1 and f2. In addition, it was reported that IDH-mutant glioblastomas occasionally include primitive neuronal components, which might contribute to the high cell density.

Tan et al reported that the intratumoral minimal ADC was significantly lower in IDH-mutant glioblastomas than in IDH-wildtype glioblastomas,[4] and their finding is consistent with our result for the f1. In contrast, Xing et al[6] and Hong et al[5] reported that IDH-wildtype glioblastomas had higher ADCs than the IDH-mutant glioblastomas. Since IDH-mutant glioblastomas develop by malignant progression from lower-grade diffuse astrocytomas, their cell density might vary depending on the amount of residual background lower-grade components containing the microcystic structures that are frequently identified in IDH-mutant lower-grade astrocytomas.[18] The discrepancy in ADC results among these studies might also be due to the small sample size for IDH-mutant glioblastoma in each study (10–18 patients).

Regarding perfusion, IDH-wildtype glioblastomas are generally hypervascular tumors that have rich neovascularization.[16] In contrast, since IDH-mutant tumors are usually a secondary tumor developing from a lower-grade glioma, the neovascularization has not been established yet during the course of the development. Investigations using dynamic susceptibility contrast perfusion-weighted imaging[6] and arterial spin labeling imaging[7] demonstrated that IDH-wildtype glioblastomas showed increased perfusion compared to IDH-mutant glioblastomas,

Table 2. ROC analysis for diagnostic performance of the parameters in the differentiation between IDH-mutant and -wildtype glioblastomas

Parameter	AUC	Sensitivity %	Specificity %	Cut-off value
κ	0.673	72.2	66.7	2.345
θ	0.552	70.4	50.0	1.006×10^{-3} mm^2/s
f1	0.753	74.1	75.0	0.430
f2	0.698	48.1	91.7	0.526
f3	0.676	74.1	58.3	0.103
ADC	0.733	70.4	75.0	1.091×10^{-3} mm^2/s

ADC, apparent diffusion coefficient; AUC, area under the curve; GB, glioblastoma; IDH, isocitrate dehydrogenase; ROC, receiver operating characteristic; f, perfusion fraction.

Figure 6. The correlations among the GD model-derived parameters and the ADC. Very strong negative correlations between f1 and the ADC were observed in both the IDH-mutant and -wildtype groups. Very strong and strong positive correlations between f2 and the ADC were observed in the IDH-mutant and IDH-wildtype groups, respectively. A weak positive correlation between f3 and ADC was observed in the IDH-wildtype group, whereas no significant correlation was observed in the IDH-mutant group. ADC, apparent diffusion coefficient; GD, γ distribution; IDH, isocitrate dehydrogenase.

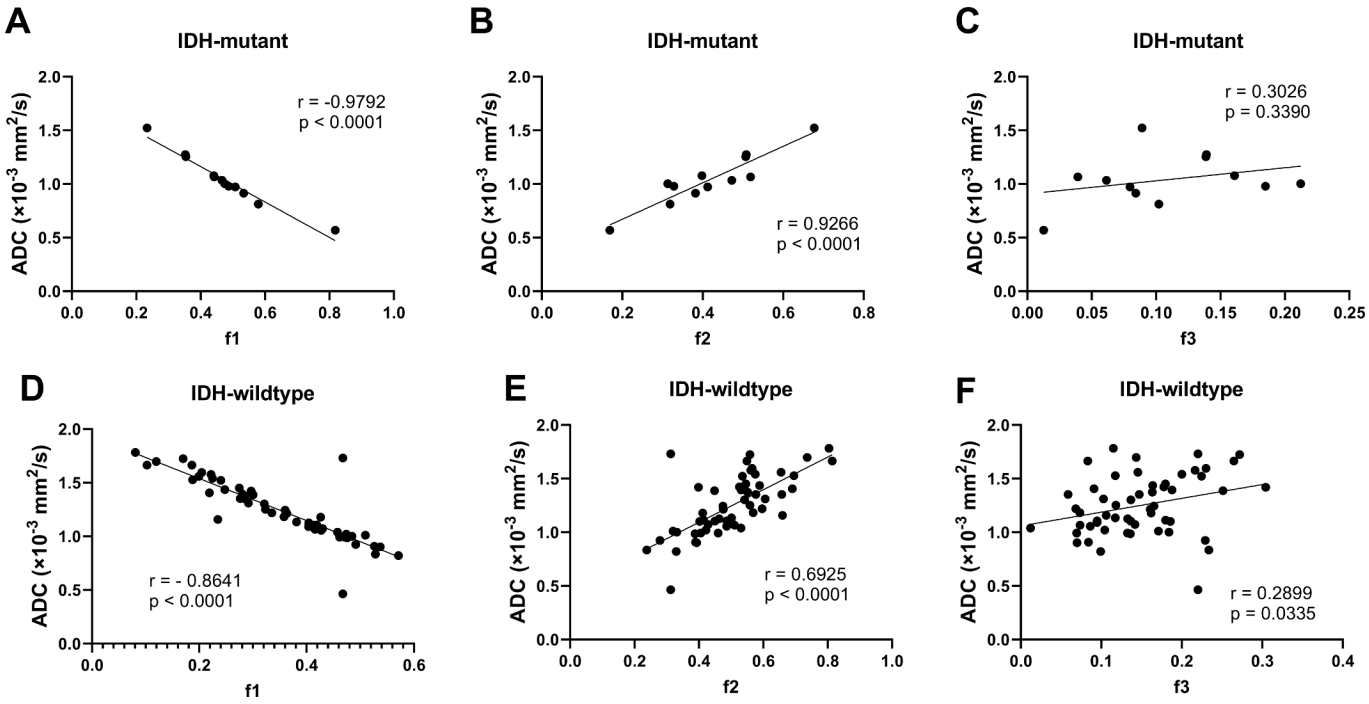

which is consistent with our result for the f3. These imaging findings are also well consistent with the results of a histologic study using CD34 immunohistochemical staining; the microvessel densities were decreased in IDH-mutated gliomas compared to IDH-wildtype gliomas.[19] The authors of that study suggested that IDH mutations could reduce the pericyte coverage of microvessels in astrocytic tumors by inhibiting the expression of angiogenesis factors.[19]

The negative correlation between the ADC and f1 and the positive correlation between the ADC and f2 probably reflect the tissue cell density and microscopic necrosis, respectively. The weak correlation between the ADC and f3 observed only in the IDH-wildtype might be due to a perfusion effect included in the ADC, which could be larger in more highly perfused IDH-wildtype glioblastomas compared to IDH-mutant glioblastomas.

In the peritumoral T2-hyperintense lesions without contrast enhancement, no significant differences were observed between the IDH-mutant and -wildtype groups for any of the parameters. This result is not in accord with MRI studies that showed the IDH-wildtype glioblastomas showed larger blood volume[6] or smaller ADCs[5] in peritumoral non-enhancing T2-hyperintense lesions compared to the IDH-mutant glioblastomas. The high f2 values in both IDH-mutant and -wildtype tumors are likely to reflect mostly perifocal vasogenic edema rather than tumor infiltration outside the enhancing lesion.

The GD model has advantages over the monoexponential model and intravoxel incoherent motion model. First, the fitting to obtain two unknowns, κ and θ, is less susceptible to fitting errors compared to the intravoxel incoherent motion model (which handles three unknowns), and thus the GD model requires less b-values. The three fractions (f1, f2, f3) obtained with this model are more practical and easily comprehensible for understanding the histopathological features of brain tumors compared to the other models.

Evaluation of morphological characteristics by conventional MRI is also useful in predicting IDH-mutation status in GM. Yamashita et al reported that the percentage of necrotic areas in enhancing lesions was related to IDH-mutation status,[7] and Wang et al reported that the incidence of enhancing effects was lower in the IDH-mutant group than in the IDH-wildtype group (IDH-mutant, 73.3%; IDH-wildtype, 94.9%, $p < 0.001$).[20] Similar to these findings, a larger proportion of non-contrast-enhancing tumor has been associated with IDH mutation status. Carrillo demonstrated that a higher percentage of the non-contrast-enhancing tumor was shown to correlate with IDH mutation status.[21] Patel et al found that fluid attenuation in non-contrast-enhancing tumors is a marker for IDH-mutant glioblastomas.[22] In addition to morphological evaluation by conventional MRI, quantitative evaluation by the GD model could be combined to further improve the diagnostic performance of IDH mutation in glioblastomas.

For this study, we used glioma nomenclature from the 2016 WHO classification ("glioblastoma, IDH-wildtype" and "glioblastoma, IDH-mutant"). However, the new the 2021 WHO classification reclassifies IDH-mutant and IDH-wildtype diffuse astrocytomas.[23] For the diagnosis of glioblastoma, IDH-wildtype, WHO Grade 4, an IDH wildtype diffusely infiltrating astrocytic glioma requires microvascular proliferation and/or necrosis and/or at least one of the following genetic alterations: telomerase reverse transcriptase (TERT) promoter mutation, epidermal growth factor receptor (EGFR) amplification, or chromosome, 7 gain/10 loss. The category of astrocytoma, IDH-mutant now includes WHO Grade 2–4 tumors. Astrocytoma, IDH-mutant, WHO Grade 4 includes diffusely infiltrating astrocytic gliomas that exhibit microvascular proliferation and/or necrosis and/or cyclin-dependent kinase inhibitor (CDKN) 2A/B homozygous deletion. The term "glioblastoma, IDH-mutant" is to be discontinued, with such cases subsumed under the category "astrocytoma, IDH-mutant, WHO Grade 4." The timing of the present study was difficult as it was performed just before the WHO classification update. The classification of tumors in this study was based on WHO 2016. Therefore, the "glioblastoma, IDH-wildtype" group did not include so-called "molecular glioblastoma", which is histologically graded 2–3 and has TERT mutation, EGFR amplification or chromosome, 7 gain/10 loss. The "glioblastoma, IDH-mutant" group did not include histologically Grade 2–3 glioblastomas with CDKN2A/B homozygous deletion.

Our study has several limitations. First, the number of patients was relatively small, especially for the patients with IDH-mutant glioblastomas (n = 12). Second, we excluded lesions that showed no distinct contrast enhancement, since we focused on the enhancing area in this study because we thought that it was the core of a tumor and should have reflected well the pathologic grade of the tumor. However, IDH-mutant astrocytomas are often not enhancing even if they are Grade 4. In addition, sometimes IDH-wildtype glioblastomas can be seen as unenhanced tumors. Third, the ROI placements on the gadolinium-enhancing lesions were occasionally difficult, particularly when the lesions showed irregular and thin ring-like enhancement. Although the best effort was made to include only enhancing lesions, it is possible that necrosis in tumors was included, and this could have affected the analyses. In addition, the selection of b-values has not yet been optimized. Because the non-monoexponential diffusion signal decay generally becomes more obvious over more extended b-value ranges, the maximum b-value of 1000 sec/mm^2 used in herein might be lower than the optimal value. The optimal b-values and numbers should be elucidated in future studies. Finally, in this study, we did not examine the pathology in detail. We hope to investigate the direct comparison between the parameters of the GD model and the pathological findings in future studies.

CONCLUSION

We confirmed that diffusion MRI based on the GD model could well describe the pathological features of IDH-mutant and -wild-type glioblastomas, and its use enabled the significant differentiation of these tumors. The f1 value was significantly larger and the f2 and f3 values were significantly smaller in the IDH-mutant glioblastomas than in the IDH-wildtype glioblastomas. The GD model may therefore contribute to the non-invasive identification of the IDH mutation status based on histological viewpoint.

FUNDING

This work was supported by a JSPS KAKENHI grant, no. JP17K10410 and JP20K08111.

REFERENCES

1. Ostrom QT, Gittleman H, Liao P, Rouse C, Chen Y, et al. CBTRUS statistical report: primary brain and central nervous system tumors diagnosed in the united states in 2007-2011. *Neuro Oncol* 2014; **16 Suppl 4**: iv1-63. https://doi.org/10.1093/neuonc/nou223
2. Louis DN, Perry A, Reifenberger G, von Deimling A, Figarella-Branger D, et al. The 2016 world health organization classification of tumors of the central nervous system: a summary. *Acta Neuropathol* 2016; **131**: 803–20. https://doi.org/10.1007/s00401-016-1545-1
3. Parsons DW, Jones S, Zhang X, Lin JC-H, Leary RJ, et al. An integrated genomic analysis of human glioblastoma multiforme. *Science* 2008; **321**: 1807–12. https://doi.org/10.1126/science.1164382
4. Tan WL, Huang WY, Yin B, Xiong J, Wu JS, et al. Can diffusion tensor imaging noninvasively detect idh1 gene mutations in astrogliomas? a retrospective study of 112 cases. *AJNR Am J Neuroradiol* 2014; **35**: 920–27. https://doi.org/10.3174/ajnr.A3803
5. Hong EK, Choi SH, Shin DJ, Jo SW, Yoo R-E, et al. Radiogenomics correlation between mr imaging features and major genetic profiles in glioblastoma. *Eur Radiol* 2018; **28**: 4350–61. https://doi.org/10.1007/s00330-018-5400-8
6. Xing Z, Zhang H, She D, Lin Y, Zhou X, et al. IDH genotypes differentiation in glioblastomas using dwi and dsc-pwi in the enhancing and peri-enhancing region. *Acta Radiol* 2019; **60**: 1663–72. https://doi.org/10.1177/0284185119842288
7. Yamashita K, Hiwatashi A, Togao O, Kikuchi K, Hatae R, et al. MR imaging-based analysis of glioblastoma multiforme: estimation of idh1 mutation status. *AJNR Am J Neuroradiol* 2016; **37**: 58–65. https://doi.org/10.3174/ajnr.A4491
8. Oshio K, Shinmoto H, Mulkern RV. Interpretation of diffusion mr imaging data using a gamma distribution model. *Magn Reson Med Sci* 2014; **13**: 191–95. https://doi.org/10.2463/mrms.2014-0016
9. Shinmoto H, Oshio K, Tamura C, Soga S, Okamura T, et al. Diffusion-weighted imaging of prostate cancer using a statistical model based on the gamma distribution. *J Magn Reson Imaging* 2015; **42**: 56–62. https://doi.org/10.1002/jmri.24761
10. Tomita H, Soga S, Suyama Y, Ito K, Asano T, et al. Analysis of diffusion-weighted mr images based on a gamma distribution model to differentiate prostate cancers with different gleason score. *Magn Reson Med Sci*

2020; **19**: 40–47. https://doi.org/10.2463/mrms.mp.2018-0124

11. Borlinhas F, Loução R, C Conceição R, Ferreira HA. Gamma distribution model in the evaluation of breast cancer through diffusion-weighted mri: a preliminary study. *J Magn Reson Imaging* 2019; **50**: 230–38. https://doi.org/10.1002/jmri.26599
12. Togao O, Chikui T, Tokumori K, Kami Y, Kikuchi K, et al. Gamma distribution model of diffusion mri for the differentiation of primary central nerve system lymphomas and glioblastomas. *PLoS One* 2020; **15**(12): e0243839. https://doi.org/10.1371/journal.pone.0243839
13. Fuller GN, Hess KR, Rhee CH, Yung WKA, Sawaya RA, et al. Molecular classification of human diffuse gliomas by multidimensional scaling analysis of gene expression profiles parallels morphology-based classification, correlates with survival, and reveals clinically-relevant novel glioma subsets. *Brain Pathol* 2002; **12**: 108–16. https://doi.org/10.1111/j.1750-3639.2002.tb00427.x
14. El Khouli RH, Macura KJ, Barker PB, Habba MR, Jacobs MA, et al. Relationship of temporal resolution to diagnostic performance for dynamic contrast enhanced mri of the breast. *J Magn Reson Imaging* 2009; **30**: 999–1004. https://doi.org/10.1002/jmri.21947
15. DeLong ER, DeLong DM, Clarke-Pearson DL. Comparing the areas under two or more correlated receiver operating characteristic curves: a nonparametric approach. *Biometrics* 1988; **44**: 837–45. https://doi.org/10.2307/2531595
16. Louis DN, Ohgaki H, Wiestler OD, Cavenee WK. *WHO Classification of Tumours of the Central Nervous System, Revised*. Fourth Edition. Lyon: IARC Press; 2016.
17. Nobusawa S, Watanabe T, Kleihues P, Ohgaki H. IDH1 mutations as molecular signature and predictive factor of secondary glioblastomas. *Clin Cancer Res* 2009; **15**: 6002–7. https://doi.org/10.1158/1078-0432.CCR-09-0715
18. Patel SH, Poisson LM, Brat DJ, Zhou Y, Cooper L, et al. T2-flair mismatch, an imaging biomarker for idh and 1p/19q status in lower-grade gliomas: a tcga/tcia project. *Clin Cancer Res* 2017; **23**: 6078–85. https://doi.org/10.1158/1078-0432.CCR-17-0560
19. Sun C, Zhao Y, Shi J, Zhang J, Yuan Y, et al. Isocitrate dehydrogenase1 mutation reduces the pericyte coverage of microvessels in astrocytic tumours. *J Neurooncol* 2019; **143**: 187–96. https://doi.org/10.1007/s11060-019-03156-5
20. Wang K, Wang Y, Fan X, Wang J, Li G, et al. Radiological features combined with idh1 status for predicting the survival outcome of glioblastoma patients. *Neuro Oncol* 2016; **18**: 589–97. https://doi.org/10.1093/neuonc/nov239
21. Carrillo JA, Lai A, Nghiemphu PL, Kim HJ, Phillips HS, et al. Relationship between tumor enhancement, edema, idh1 mutational status, mgmt promoter methylation, and survival in glioblastoma. *AJNR Am J Neuroradiol* 2012; **33**: 1349–55. https://doi.org/10.3174/ajnr.A2950
22. Patel SH, Batchala PP, Muttikkal TJE, Ferrante SS, Patrie JT, et al. Fluid attenuation in non-contrast-enhancing tumor (ncet): an mri marker for isocitrate dehydrogenase (idh) mutation in glioblastoma. *J Neurooncol* 2021; **152**: 523–31. https://doi.org/10.1007/s11060-021-03720-y
23. Louis DN, Perry A, Wesseling P, Brat DJ, Cree IA, et al. The 2021 who classification of tumors of the central nervous system: a summary. *Neuro Oncol* 2021; **23**: 1231–51. https://doi.org/10.1093/neuonc/noab106